CrystEngComm

Accepted Manuscript

ROYAL SOCIETY OF CHEMISTRY

www.rsc.org/crystengcomm

Two series of pH-dependent lanthanide coordination polymers demonstrating solvent-induced single crystal to single crystal transformation, sorption and luminescent properties†

Lina Zhang,[a,b] Chao Zhang,[a] Bin Zhang,[a] Chenxia Du,*[a] and Hongwei Hou*[a]

[a] *College of Chemistry and Molecular Engineering, Zhengzhou University, Zhengzhou, 450052, P. R. China.*

[b] *College of Physics and Chemistry, Henan Polytechnic University, Jiaozuo 454000, P. R. China.*

E-mail: dcx@zzu.edu.cn, houhongw@zzu.edu.cn.

Abstract: Two series of new lanthanide coordination polymers have been obtained by the solvothermal reaction of $Ln(NO_3)_3$ and pamoic acid under different pH values. Both series of compounds show three-dimensional porous frameworks composed of dinuclear Ln(III) subunits. Series B demonstrate fascinating solvent-induced dynamic behaviors in SCSC (Single Crystal to Single Crystal) manner. The capability of activated series B to absorb liquid acetone was investigated by means of ^1H NMR spectroscopy, demonstrating the potential of Ln-MOFs as highly efficient and reusable liquid acetone sorbents. In addition, photoluminescence properties of Nd (**3**), Eu (**5**) and Yb (**10**) were measured and discussed. Lanthanide contraction effect also played a crucial role in the formation of each series of complexes. Analysis of the relations between ionic radius (Ln^{3+}) and the number of f electrons in these complexes indicates that lanthanide contraction effect in both series can be well described by Raymond model.

1. Introduction

Porous coordination polymers (PCPs) have attracted vast attention in recent years due to their potential applications in diverse fields, such as gas storage/separations, [1-5] drug delivery, [6-8] catalysis, [9-11] luminescence, [12-13] sensing [14] and selective encapsulation of guest molecules. [15-19] Dynamic PCPs (soft porous crystals) are of very important category of the PCPs due to that they can modulate their pore size and properties and reversibly switched between open and closed forms, generally triggered by external stimuli such as temperature, pressure or guest sorption. [20-21] As a result, the dynamic properties of these materials make them very useful for applications in high selectivity or gated adsorption/desorption behavior for guest solvents. [22-26]

Instances for dynamic behaviors of the soft PCPs obtained by solvent-induced single-crystal to single-crystal (SCSC) transformations based on transition metals have been widely reported. [27-31] However, there are only very limited examples of lanthanide (Ln) based soft PCPs were utilized to investigate the dynamic behaviors through the SCSC transformations. [32-33] This is mainly due to the difficulty in synthesizing soft porous Ln-MOFs: the large coordination sphere and flexible coordination geometry of lanthanide ions lead to the formation of either condensed frameworks or only "structurally porous" frameworks which are readily collapsed once the terminal and free solvent molecules are removed during the activation. [34] Furthermore, it is challenging to obtain high quality crystals after solid state transformations, especially those involving changes in the coordination environment of lanthanide ions. This could be due to breaking and formation of new coordination bonds which causes loss of the long-range structural order of the crystals.[35-37]

Lanthanides, with special luminescent [38] and magnetic [39] properties originating from their 4f electrons, are always used to construct functional complexes with unique properties and desired features. [40] In our previous work, the porous coordination polymer $\{[Dy_2(PA)_3(H_2O)_2(DMF)_2]\cdot(DMF)_3\cdot(H_2O)\}_n$ (**11a**) with interesting magnetic properties was obtained by using a semi-flexible dicarboxylic acid, pamoic acid. [41a] To the best of our knowledge, there are only very

limited lanthanide complexes based on pamoic acid have been found, [41] and no lanthanide dynamic PCPs based on pamoic acid have been reported so far.

Herein, two series of new Ln-MOFs with the general formulas $\{[Ln_2(PA)_3(H_2O)_{4-x}(DMF)_x]\cdot(DMF)_2\cdot(H_2O)_y\}_n$ (x=2, y=0, Ln = Ce (**1**); x=1.5, y=0, Ln = Pr (**2**), Nd (**3**) Sm (**4**), Eu (**5**), Gd (**6**), Tb (**7**); x=1, y=1, Ln = Ho (**8**), Er (**9**), Yb (**10**)) [series A] and $\{[Ln_2(PA)_3(H_2O)_2(DMF)_2]\cdot(DMF)_3\cdot(H_2O)\}_n$ (Ln = Tb (**7a**), Ho (**8a**), Er (**9a**), Yb (**10a**)) [series B] (H_2PA = pamoic acid, 4,4′-methylenebis[3-hydroxy-2-naphthalenecarboxylic acid]) were produced by the solvothermal reaction of $Ln(NO_3)_3$ and pamoic acid under different pH values. Series B was observed to demonstrate fascinating solvent-induced dynamic behaviors in SCSC manner. The capability of activated series B to absorb liquid acetone was studied by means of ^{1}H NMR spectroscopy, demonstrating the potential of Ln-MOFs as highly efficient and reusable liquid acetone sorbents. Moreover, the solid-state photoluminescence properties of selected compounds in series A were measured and discussed. In addition, lanthanide contraction effect in both series was well described by Raymond model.

2. Experimental section

2.1 Materials and physical measurements

The $Ln(NO_3)_3\cdot6H_2O$ (Ln = Ce, Pr, Nd, Sm, Eu, Gd, Tb, Ho, Er, and Yb) were prepared by dissolving the corresponding rare earth oxides in an aqueous solution of HNO_3 (6.0 M) while adding a bit of H_2O_2 for Tb_4O_7 and then were evaporated at 100 °C. The other chemicals purchased were of reagent grade and used without further purification. The IR spectra were recorded on a BRUKER TENSOR 27 spectrophotometer with KBr pellets in the region of 400−4000 cm^{-1}. Elemental analyses of C, H, and N were performed on a Flash EA 1112 elemental analyzer. Thermal analysis was performed on a Netzsch STA 449C thermal analyzer at a heating rate of 10 °C/min in air. Room-temperature powder X-ray diffraction data (PXRD) were recorded using CuKα radiation on a PANalytical X'Pert PRO diffractometer. Luminescent spectra were recorded on a FluoroMax@-P spectrophotometer at room temperature. ^{1}H NMR spectra were obtained using a Bruker DPX-400 MHz spectrometer in $CDCl_3$.

2.2 Synthesis of the compounds

$\{[Ln_2(PA)_3(H_2O)_{4-x}(DMF)_x]\cdot(DMF)_2\cdot(H_2O)_y\}_n$ (1-10). Starting materials of $Ln(NO_3)_3$ (0.1 mmol) (Ln = Ce, Pr, Nd, Sm, Eu, Gd, Tb, Ho, Er, and Yb) and H_2PA (0.1 mmol) were dissolved in a mixed solvent of H_2O (6 mL) and DMF (4 mL). The pH value of the solution was adjusted to the range of 6.0-7.0 by adding 0.5 $mol\cdot L^{-1}$ NaOH aqueous solution. Then the mixture was placed in a Teflon-lined stainless steel vessel and heated at 110 °C for 72 h. After cooling slowly down to room temperature at 5 °C/h, crystals of **1-10** were collected and dried in air.

$\{[Ce_2(PA)_3(H_2O)_2(DMF)_2]\cdot(DMF)_2\}_n$ (**1**). Elem. anal. Calcd (%) for $C_{81}H_{74}Ce_2N_4O_{24}$ (Mr = 1767.63): C, 54.99; H, 4.19; N, 3.17. Found: C, 55.03; H, 4.24; N, 3.22. IR (KBr, cm^{-1}): 3421(b), 3062(w), 2934(w), 1649(vs), 1538(w), 1458(m), 1399(s), 1234(w), 1094(w), 811(w), 752(w).

$\{[Pr_2(PA)_3(H_2O)_{2.5}(DMF)_{1.5}]\cdot(DMF)_2\}_n$ (**2**). Elem. anal. Calcd (%) for $C_{79.5}H_{71.5}N_{3.5}O_{24}Pr_2$ (Mr = 1741.66): C, 54.78; H, 4.11; N, 2.81. Found: C, 54.83; H, 4.17; N, 2.78. IR (KBr, cm^{-1}): 3422(b), 3060(w), 2932(w), 1647(vs), 1536(w), 1456(m), 1397(s), 1232(w), 1096(w), 811(w), 752(w).

$\{[Nd_2(PA)_3(H_2O)_{2.5}(DMF)_{1.5}]\cdot(DMF)_2\}_n$ (**3**). Elem. anal. Calcd (%) for $C_{79.5}H_{71.5}N_{3.5}Nd_2O_{24}$ (Mr = 1748.31): C, 54.57; H, 4.09; N, 2.80. Found: C, 54.67; H, 4.06; N, 2.83. IR (KBr, cm^{-1}): 3421(b), 3060(w), 2932(w), 1649(vs), 1536(w), 1458(m), 1396(s), 1230(w), 1092(w), 809(w), 752(w).

$\{[Sm_2(PA)_3(H_2O)_{2.5}(DMF)_{1.5}]\cdot(DMF)_2\}_n$ (**4**). Elem. anal. Calcd (%) for $C_{79.5}H_{71.5}N_{3.5}O_{24}Sm_2$ (Mr = 1760.55): C, 54.19; H, 4.06; N, 2.78. Found: C, 54.26; H, 4.03; N, 2.76. IR (KBr, cm^{-1}): 3420(b), 3062(w), 2935(w), 1647(vs), 1536(w), 1458(m), 1399(s), 1231(w), 1094(w), 811(w), 753(w).

$\{[Eu_2(PA)_3(H_2O)_{2.5}(DMF)_{1.5}]\cdot(DMF)_2\}_n$ (**5**). Elem. anal. Calcd (%) for $C_{79.5}H_{71.5}Eu_2N_{3.5}O_{24}$ (Mr =1763.79): C, 54.09; H, 4.05; N, 2.78. Found: C, 54.06; H, 4.01; N, 2.72. IR (KBr, cm^{-1}): 3421(b), 3060(w), 2932(w), 1647(vs), 1536(w), 1458(m), 1397(s), 1232(w), 1092(w), 811(w), 752 (w).

$\{[Gd_2(PA)_3(H_2O)_{2.5}(DMF)_{1.5}]\cdot(DMF)_2\}_n$ (**6**). Elem. anal. Calcd (%) for $C_{79.5}H_{71.5}Gd_2N_{3.5}O_{24}$ (Mr = 1774.35): C, 53.77; H, 4.03; N, 2.76. Found: C, 53.80; H, 4.06; N, 2.74. IR (KBr, cm^{-1}): 3420(b), 3060(w), 2931(w), 1646(vs), 1534(w), 1456(m), 1397(s), 1232(w), 1092(w), 812(w), 750(w).

$\{[Tb_2(PA)_3(H_2O)_{2.5}(DMF)_{1.5}]\cdot(DMF)_2\}_n$ (**7**). Elem. anal. Calcd (%) for $C_{79.5}H_{71.5}N_{3.5}O_{24}Tb_2$ (Mr = 1777.19): C, 53.68; H, 4.02; N, 2.76. Found: C, 53.72; H, 4.05; N, 2.73. IR (KBr, cm^{-1}): 3421(b), 3060(w), 2934(w), 1649(vs), 1538(w), 1458(m), 1397(s), 1234(w), 1096(w), 811(w), 752(w).

$\{[Ho_2(PA)_3(H_2O)_3(DMF)]\cdot(DMF)_2\cdot(H_2O)\}_n$ (**8**). Elem. anal. Calcd (%) for $C_{78}H_{71}Ho_2N_3O_{25}$ (Mr = 1780.22): C, 52.58; H, 3.99; N, 2.36. Found: C, 52.68; H, 4.03; N, 2.39. IR (KBr, cm^{-1}): 3420(b), 3062(w), 2932(w), 1646(vs), 1538(w), 1458(m), 1397(s), 1234(w), 1096(w), 811(w), 752 (w).

$\{[Er_2(PA)_3(H_2O)_3(DMF)]\cdot(DMF)_2\cdot(H_2O)\}_n$ (**9**). Elem. anal. Calcd (%) for $C_{78}H_{71}Er_2N_3O_{25}$ (Mr =1784.88): C, 52.44; H, 3.98; N, 2.35. Found: C, 52.48; H, 4.06; N, 2.40. IR (KBr, cm^{-1}): 3421(b), 3060(w), 2931(w), 1647(vs), 1534(w), 1456(m), 1397(s), 1233(w), 1092(w), 811(w), 752(w).

$\{[Yb_2(PA)_3(H_2O)_3(DMF)]\cdot(DMF)_2\cdot(H_2O)\}_n$ (**10**). Elem. anal. Calcd (%) for $C_{78}H_{71}N_3O_{25}Yb_2$ (Mr =1796.43): C, 52.10; H, 3.95; N, 2.34. Found: C, 52.22; H, 4.01; N, 2.36. IR (KBr, cm^{-1}): 3421(b), 3060(w), 2934(w), 1647(vs), 1538(w), 1456(m), 1399(s), 1234(w), 1092(w), 811(w), 752(w)

$\{[Ln_2(PA)_3(H_2O)_2(DMF)_2]\cdot(DMF)_3\cdot(H_2O)\}_n$ (7a–10a). Complexes **7a–10a** were obtained by the same synthetic procedure of complexes **1–10** except that the pH value of the starting materials was adjusted to the range of 2.0-5.0 with 0.5 mol· L^{-1} hydrochloric acid aqueous solution. Lamellar crystals of **7a–10a** were obtained.

$\{[Tb_2(PA)_3(H_2O)_2(DMF)_2]\cdot(DMF)_3\cdot(H_2O)\}_n$ (**7a**) Elem. anal. Calcd (%) for $C_{84}H_{83}Tb_2N_5O_{26}$ (Mr = 1896.38): C, 53.15; H, 4.38; N, 3.69. Found: C, 53.58; H, 4.41; N, 3.74. IR (KBr, cm^{-1}): 3416(b), 3056(w), 2927(w), 1645(vs), 1457(m), 1394(s), 1204(w), 1098(w), 812(w), 749(w).

$\{[Ho_2(PA)_3(H_2O)_2(DMF)_2]\cdot(DMF)_3\cdot(H_2O)\}_n$ (**8a**) Elem. anal. Calcd (%) for $C_{84}H_{83}Ho_2N_5O_{26}$ (Mr = 1908.35): C, 52.82; H, 4.35; N, 3.67. Found: C, 53.15; H, 4.34; N, 3.72. IR (KBr, cm^{-1}): 3419(b), 3056(w), 2927(w), 1645(vs), 1457(m), 1394(s), 1202(w), 1096(w), 812(w), 747(w).

$\{[Er_2(PA)_3(H_2O)_2(DMF)_2]\cdot(DMF)_3\cdot(H_2O)\}_n$ (**9a**) Elem. anal. Calcd (%) for $C_{84}H_{83}Er_2N_5O_{26}$ (Mr = 1913.06): C, 52.69; H, 4.34; N, 3.66. Found: C, 53.02; H, 4.28; N, 3.73. IR (KBr, cm^{-1}): 3416(b), 3055(w), 2927(w), 1644(vs), 1457(m), 1394(s), 1202(w), 1096(w), 812(w), 748(w).

$\{[Yb_2(PA)_3(H_2O)_2(DMF)_2]\cdot(DMF)_3\cdot(H_2O)\}_n$ (**10a**) Elem. anal. Calcd (%) for $C_{84}H_{83}Yb_2N_5O_{26}$ (Mr = 1924.62): C, 52.37; H, 4.31; N, 3.64. Found: C, 52.88; H, 4.27; N, 3.69. IR (KBr, cm^{-1}): 3416(b), 3054(w), 2927(w), 1645(vs), 1459(m), 1396(s), 1202(w), 1096(w), 812(w), 749(w).

Solvent-exchanged compounds in SCSC manner. The acetone-exchanged compound **8a/acetone** was obtained by immersing crystals of **8a** in acetone at room temperature for 2 days. The solvent-free material **8a/dry** was obtained by heating compound **8a/acetone** at 70 °C under vacuum for 12 hours. The water-absorbed compound **8a/H_2O** was obtained by placing compound **8a/dry** in the air for 48 hours. The alcohol-exchanged compound **8a/EtOH** was obtained by placing crystals of **8a** in alcohol at room temperature for 7 days.

$\{[Ho_2(PA)_3(H_2O)_4]\cdot(acetone)_2\cdot(H_2O)_3\}_n$ (**8a/acetone**) Elem. anal. Calcd (%) for $C_{75}H_{68}O_{27}Ho_2$ (Mr = 1731.09): C, 51.99; H, 3.93. Found: C, 51.81; H, 3.91.

$\{[Ho_2(PA)_3(H_2O)_4]\}_n$ (**8a/dry**). Elem. anal. Calcd (%) for $C_{69}H_{50}Ho_2O_{22}$ (Mr = 1560.95): C, 53.04; H, 3.20. Found: C, 52.84; H, 3.18.

Scheme 1. Synthetic strategy of compounds **1-10** and **7a-10a.**

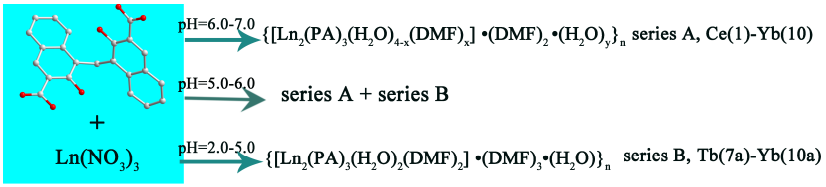

$\{[Ho_2(PA)_3(H_2O)_4]\cdot(H_2O)_9\}_n$ (**8a/H$_2$O**). Elem. anal. Calcd (%) for $C_{69}H_{68}Ho_2O_{31}$ (Mr = 1722.95): C, 48.06; H, 3.95. Found: C, 47.83; H, 3.90.

$\{[Ho_2(PA)_3(H_2O)_2(EtOH)_2]\cdot(H_2O)_4\cdot(DMF)_2\}_n$ (**8a/EtOH**). Elem. anal. Calcd (%) for $C_{79}H_{78}Ho_2N_2O_{28}$ (Mr = 1833.23): C, 51.71; H, 4.25; N, 1.53. Found: C, 51.60; H, 4.22; N, 1.48

2.3 Crystal data collection and refinement

Crystallographic data collections for all the complexes were carried out on an Oxford Diffraction Xcalibur CCD diffractometer with graphite-monochromated Mo-Kα (λ = 0.71073Å) or Cu-Kα (λ = (1.5418 Å) radiation at 293(2) K using the ω-scan technique. The structures were obtained by the direct methods using the program SHELXS-97 and all non-hydrogen atoms except for some water and DMF molecules were refined anisotropically on F^2 by the full-matrix least-squares technique which used the SHELXL-97 crystallographic software package. [42-43] The hydrogen atoms were placed at calculated positions and refined as riding atoms with isotropic displacement parameters. No hydrogen atoms associated with water molecules were located from the difference Fourier map. In the structure, some free solvent molecules were highly disordered, and attempts to locate and refine the solvent peaks were not successful. The SQUEEZE program was used to remove scattering from the highly disordered water and DMF molecules. The final chemical formulas of these compounds were calculated from the Crystallographic data combined with the TGA and elemental analysis data. The crystallographic crystal data and structure processing parameters for compounds **1–10**, **8a–10a**, **8a/acetone**, **8a/EtOH**, **8a/dry** and **8a/H$_2$O** are summarized in Tables S1-S4 in the Supporting Information. Selected bond lengths are listed in Tables S5-S6. As for compound **7a,** only cell parameters are given in Table S3 due to its poor crystal quality. CCDC reference numbers are 1024564-1024573 for **1-10**, 1024575-1024577 for **8a-10a**, 1042634 for **8a/acetone**, 997904 for **8a/dry**, 1024578 for **8a/H$_2$O**, 1029462 for **8a/EtOH**, 1029461 for **8a/acetone** regenerated from **8a/dry**. These data can be obtained free of charge via www.ccdc.cam.ac.uk/data_request/cif

3. Results and discussion

3.1 Design and synthesis

Among the various experimental conditions in controlling the formation of the resultant structures, pH value of the reaction system was found to be the main structure-directing factor during the self-assembly process (Scheme 1). Both series of compounds were obtained simultaneously when the reactions were carried out at 110 °C in the mixed solvent of H_2O and DMF within the pH range of 5.0-6.0. At temperatures below 110 °C, all products are precipitates, suggesting that the temperature of 110 °C is a critical factor in the formation of crystals. When the reaction time was two days, tiny crystals not suitable for the single-crystal X-ray analyses were obtained. Further increase reaction time did not affect the crystalline morphology of the MOFs. When we increase the pH value of the starting materials to the range of 6.0-7.0, pure phase crystals of **1-10** and some yellow precipitates were generated, while pure phase crystals of **7a-10a** were obtained by regulating the pH values to the range of 2.0-5.0, without altering reagents. It is worth to note that although very similar reaction conditions were used to synthesize

complexes **1a-10a**, only heavy rare earth MOFs (**7a–10a**) were obtained, no perfect crystals of light and medium lanthanide MOFs (**1a−6a)** can be isolated. Although cell parameters of compound **7a** were obtained, full determination of its structure cannot be done due to the poor crystal quality. We speculated that lanthanide contraction effect results in such phenomenon.

3.2 Description of the crystal structures

$\{[Ln_2(PA)_3(H_2O)_{4-x}(DMF)_x]\cdot(DMF)_2\cdot(H_2O)_y\}_n$ (1-10)

Crystal structure determination reveals that compounds **1–10** are isostructural in nature and crystallize in the monoclinic space group $P2_1/c$. They exhibit very similar basic structures, except for the different number of coordinated water and DMF molecules in the crystal lattice (Fig. 1a-1b). As a representative example, only the structure of **8** (Ho) is described here in detail. As depicted in Fig. 1a, compound **8** contains the binuclear unit $[Ho_2(COO)_6(H_2O)_3(DMF)]$ as the secondary building unit (SBU). Each SBU comprises of two eight-coordinated Ho^{3+} centers and six $-COO^-$ groups from six PA^{2-} anions. Two Ho(III) centers are linked by four of the $-COO^-$ groups in η^1: η^1: μ_2 fashion. Each of the remaining two $-COO^-$ groups acts as chelating ligand coordinating to a single Ho^{3+} ion, respectively. The coordination sphere of Ho1 center is completed by two oxygen atoms from one DMF and one water molecules, while that of Ho2 center is completed by two oxygen atoms from two H_2O molecules. The Ho−O distances involving Ho1 and Ho2 centers are ranging from 2.303(3) to 2.465(4) Å and 2.272(4) to 2.476(3) Å, respectively. The O–Ho–O bond angles vary from 53.31(11) to 150.27(12) ° (Table S5). The Ho···Ho distance in the binuclear SBU is 4.3679(10) Å.

Interestingly, each SBU of complex **8** is linked to six adjacent SBUs by PA^{2-} anions producing an interesting configuration (Fig. S1a, ESI†), which is further bridged by the PA^{2-} anions to form a 3D **pcu** network with the binuclear unit $[Ho_2(COO)_6(H_2O)_3(DMF)]$ acting as a 6-connected node (Fig. S1b, ESI†). Notably, uncoordinated solvent molecules are filled in the 1D

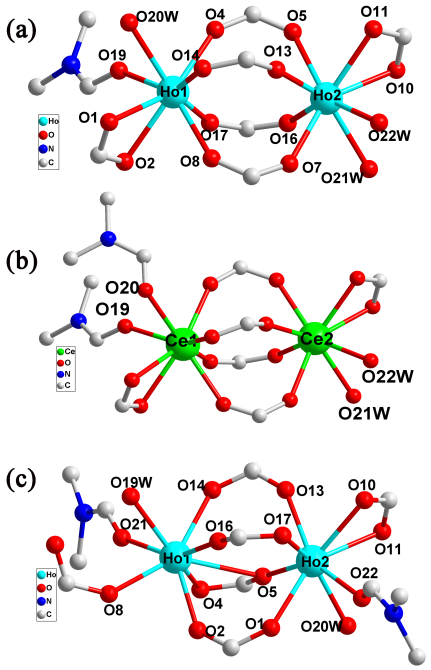

Fig.1 Representation of the binuclear SBU in (a) compound **8**, (b) compound **1** and (c) compound **8a**.

elliptic-shaped channels with the dimension of ca. 17.43 × 4.50 $Å^2$ along the *a* direction and the 1D triangular-shaped channels along the *c* direction (Fig. 2). The solvent-accessible volume of compound **8** calculated by PLATON [44] is 1112.9 $Å^3$ corresponding to 15.3% of the unit cell volume (taking into account the vander Waals radii of the atoms and excluding all solvents of the pores).

$[Ln_2(PA)_3(H_2O)_2(DMF)_2]\cdot(DMF)_3\cdot(H_2O)\}_n$ (7a–10a)

Single-crystal X-ray diffraction analysis reveals that compounds **7a–10a** are isostructural with **11a**, [41a] and thus only the structure of **8a** will be discussed in detail. Compound **8a** crystallizes in the orthorhombic space group $Pna2_1$ and contains the binuclear unit $[Ho_2(COO)_6(H_2O)_2(DMF)_2]$ as the secondary building unit (Fig. 1c). In each SBU, two eight-coordinated Ho^{3+}centers were connected by four of the $-COO^-$ groups in either η^1: η^1: μ_2 *or* η^1: η^2: μ_2 fashion. The remaining two $-COO^-$ groups act as chelating and mono-dentated ligands coordinating to a single Ho^{3+} ion, respectively. The coordination sphere of each Ho^{3+} is completed by two oxygen atoms from one DMF and one H_2O molecules. The Ho–O bond lengths are in the

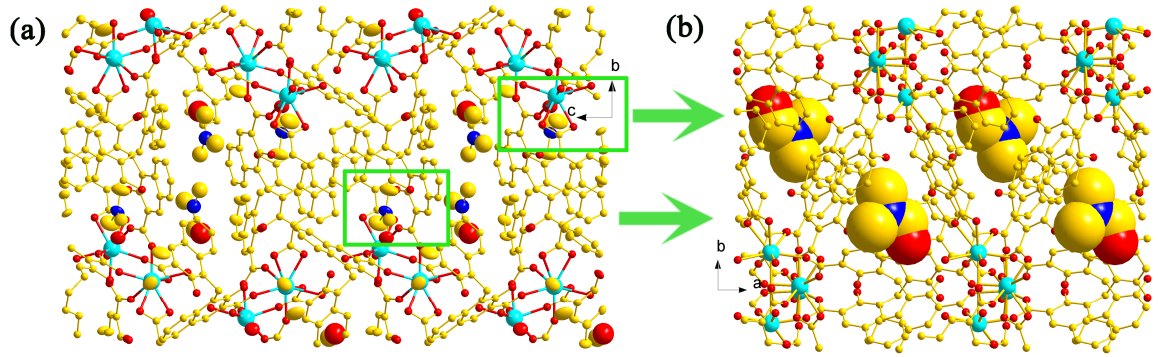

Fig.2 Illustration of the free DMF molecules filled in the channels (a) along the *a* direction; (b) along the *c* direction in **8**.

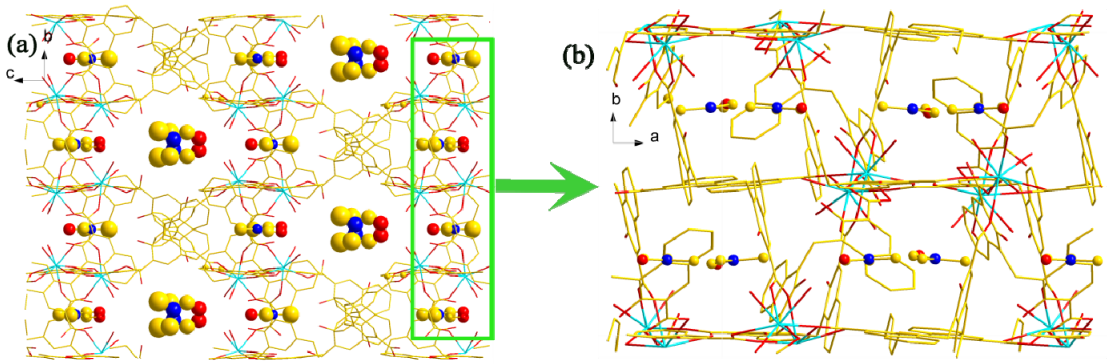

Fig. 3. Representations of the free DMF molecules filled in the channels: (a) along the *a* direction; (b) along the *c* direction in **8a**.

range of 2.254(3)–2.676(3) Å and the O–Ho–O bond angles vary from 50.59(10) to 152.58(14) ° (Table S5). The Ho···Ho distance in the binuclear unit of compound **8a** is 3.9965(3) Å.

Each SBU of **8a** is connected to six adjacent SBUs by PA^{2-} anions producing an interesting configuration (Fig. S2a, ESI†), which is further bridged by the PA^{2-} anions to form a 3D **pcu** network with the binuclear unit $[Ho_2(COO)_6(H_2O)_2(DMF)_2]$ acting as a 6-connected node (Fig. S2b, ESI†). Notably, uncoordinated DMF molecules are filled in the 1D square-shaped channels with the dimension of ca. 13.51 × 13.51 $Å^2$ along the *a* direction and the 1D channels along the *c* direction (Fig. 3). The solvent-accessible volume of compound **8a** calculated by PLATON [44] is 2350.0 $Å^3$ corresponding to 27.9% of the unit cell volume (taking into account the vander Waals radii of the atoms and excluding all solvents of the pores).

3.3 Lanthanide contraction and structural diversity

The lanthanide contraction effect is clearly observed from the decreasing trends of the unit cell volumes (Tables S1-S3†), and average Ln−O bonding distances (Table S5†) in both series from light lanthanide to heavy lanthanide. It is interesting to find that the coordination environments of Ln(III) ions in compounds **1-10** is slight differences. One of the coordination sites around Ce1 center of complex **1** is occupied by one DMF molecule (Fig. 1b), whereas 0.5 DMF and 0.5 water molecule occupies the corresponding site in **2–7,** and one water molecule occupies this site in **8–10**. This trend is related to the decrease in ionic radius from Ce(III) to Yb(III). The steric crowding in the coordination sphere increases from Ce(III) to Yb(III), and as a result small donor of water molecule replaces the relative big donor of DMF molecule to reduce the steric hindrance around the metal centers and stabilize the crystal structures.

Raymond et al. proposed that lanthanide contraction could be depicted by a linear relation between the inverse of ionic radius and the number of f electrons: $1/r(x) = a + bx$, where x is the number of f electrons in the lanthanide ion. [45] The ionic radius of Ln^{3+} ($r(x)$) in these lanthanide complexes were

obtained by subtracting the ionic radius of O^{2-} ion (1.4 Å) [46] from the Ln−O internuclear distances. In both A and B series, all the Ln−O bond distances in the dinuclear units are different. Usually, the higher denticity may cause less uniformity in the trend, while the lower denticity can grant each bond more freedom to change. [47] For this consideration, they are treated by divided into two different types: average Ln−O bonds of water and DMF molecules; average Ln−O bonds of carboxylates. For the sake of providing better evaluation of the lanthanide contraction, the Dy−O bonds length of **11a** was also taken into our consideration, due to that it is isostructural with series B. [41a] As shown in Fig. 4, good linear fits were obtained for two types of Ln−O bonds in both series. The above results illustrated that lanthanide contraction effect in both series can be well described by Raymond model. When the linear fit y = 0.0139x + 0.9184 obtained from compounds **8a-11a** were used to calculate the ionic radius of Ln^{3+} (Ce, Pr, Nd, Sm, Eu, Gd), with which we failed to get perfect crystals of series B, the data were 1.073, 1.057, 1.042, 1.012, 0.998 and 0.985 Å, respectively, which are apparently smaller than the effective ionic radius for eight-coordinate Ln^{3+} (1.143, 1.126, 1.109, 1.079, 1.066, and 1.053 Å).[47] We speculate that such difference in the ionic radius may be the main reason for the formation of poor quality crystals of these compounds.

3.4 Solvent-induced structural transformations in SCSC fashion

The presence of disordered coordinating and lattice solvent molecules in compounds **1-10** and **7a-10a** in combination with their excellent stability in air (retains their crystallinity after heating at 120 °C) prompted us to investigate their SCSC properties through a solvent exchange method. As representative example, solvent-induced dynamic behaviors of compound **8a** will be discussed systematically. The crystalline samples of **8a** of suitable size were, respectively, immersed in several solvents, namely,

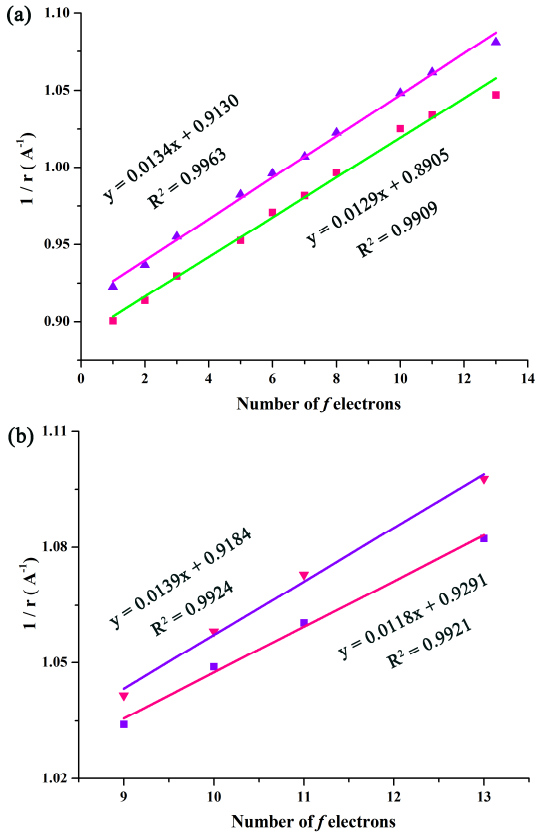

Fig. 4 Plots of the inverse of the ionic radii *vs* the number of the f electrons (a) for compounds **1-10** (green line: fitting from average Ln−O bonds length of water and DMF molecules; pink line: fitting from average Ln−O bonds length of carboxylates); (b) for compounds **8a-11a** (pink line: fitting from average Ln−O bonds length of water and DMF molecules; purple line: fitting from average Ln−O bonds length of carboxylates).

MeOH, EtOH, H_2O, acetone, acetonitrile, THF, CH_2Cl_2, diethyl ether and chloroform at room temperature. As depicted in Fig. 5, the free and coordinated DMF molecules of **8a** can be selectively exchanged by acetone/H_2O or alcohol/H_2O molecules in SCSC manner to give compound **8a**/**acetone** and **8a**/**EtOH**, respectively. Reversible SCSC transformations upon desorption/adsorption of the acetone solvents occurred in **8a**/**acetone**, generating the guest-free compound **8a**/**dry**. Interestingly, a new compound **8a**/**H_2O** was produced by placing **8a**/**dry** in the air for two days, originating from absorbing water molecules in the air.

Single crystal X-ray diffraction analysis reveals that **8a**/**acetone** still maintains the original orthorho-

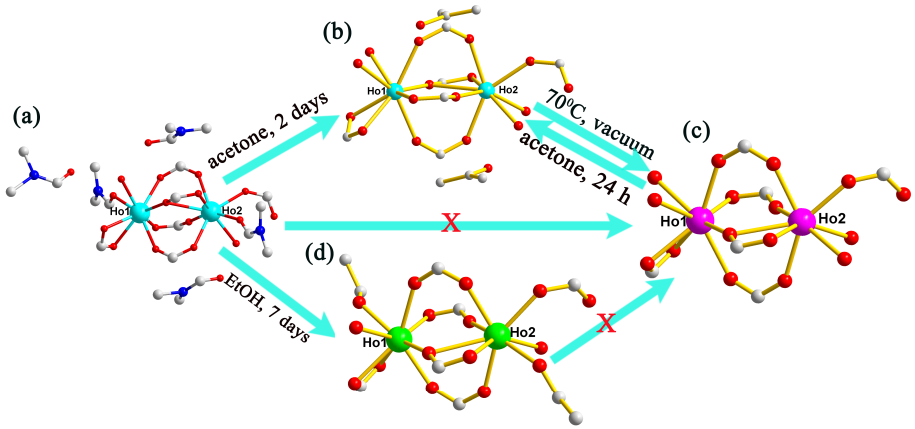

Fig. 5 SCSC transformation processes of (a) compound **8a**, (b) **8a**/**acetone**, (c) **8a**/**dry** and (d) **8a**/**EtOH**. Lattice water molecules are omitted for clarity.

mbic space group *Pna*2$_1$. Two lattice acetone and about three lattice water molecules replaced three lattice DMF molecules while two water molecules substituted two DMF molecules connected to each Ho^{3+}center (Fig. 5a, 5b), with the water molecule presumably originating from residual H_2O in the acetone solvent. Notably, the replacement of the DMF molecules by acetone/H_2O resulted in a reduction of the unit cell parameters of **8a**/**acetone**, such as *b*, *c* and volume, contracted by 3.21%, 1.31%, and 4.45%, respectively (Table S4†). Accordingly, the size of the square window of the 1D channel along the *a* direction reduced from ca.13.51 Å × 13.51 Å in **8a** to ca. 13.32 Å × 13.32 Å in **8a**/**acetone** because of the replacement of DMF by water molecules in the pore (Fig. S3†). Interestingly, two acetone molecules replaced the remaining two DMF molecules filled in the 1D channel along the *c* direction. Compared to the Ho-O_{DMF} bond distances in **8a** (2.319(4) and 2.359(3) Å), the substitution of the DMF by water molecules led to a little longer Ho-O_{water} bond distances in **8a**/acetone (2.387(6) and 2.365(5) Å) (Table S6†).

Interestingly, the solvent-free compound $\{[Ho_2(PA)_3(H_2O)_4]\}_n$ (**8a**/**dry**) was obtained by heating the acetone-exchanged compound **8a/acetone** at 70 °C under vacuum for 12 hours (Fig. 5c). In comparison with **8a**/**acetone**, the unit cell parameters of **8a**/**dry**, such as *b*, *c* and volume, slightly contracted by 0.46%, 0.45% and 0.78%, respectively. Accordingly, the size of the square window of the 1D channel along the *a* direction reduced from ca.13.32 Å × 13.32 Å to ca. 13.24 Å × 13.24 Å. It is noteworthy that the porous guest-free form (**8a**/**dry**) could not be directly obtained from **8a** by heating under a dynamic vacuum, which may be attributed to the non-volatility of the guest DMF molecule relative to the acetone solvent. As expected, when fresh solvent-free compound **8a**/**dry** was immersed in acetone at room temperature for 24 hours, it recovered to the solvent–containing form **8a**/**acetone'** (Table S4†). The reversible SCSC transformations involving free solvent via desorption/adsorption processes may find some uses in switching, sensor and reusable sorbent applications.

Strikingly, a new compound $\{[Ho_2(PA)_3(H_2O)_4]\cdot(H_2O)_9\}_n$ (**8a**/**H_2O**) was obtained by placing the guest-free compound **8a**/**dry** in the air for two days. Single crystal X-ray diffraction analysis reveals that **8a**/**H_2O** still maintains the original orthorhombic space group *Pna*2$_1$, while about nine lattice water molecules filled in its 1D channel. Compared to **8a**/**dry**, there was only a little expansion of *b* and *c* axes (Δb = 0.48%, and Δc = 0.23%), which consequently resulted in a small expansion of the cell volume (ΔV = 0.25%) (Table S4†). Accordingly, the size of the square window along the *a* direction slightly increased from ca.13.24 Å × 13.24 Å to ca. 13.26 Å × 13.26 Å (Fig. S3†).

Similarly, the alcohol-exchanged compound $\{[Ho_2(PA)_3(H_2O)_2(EtOH)_2]\cdot(H_2O)_4\cdot(DMF)_2\}_n$

(**8a**/**EtOH**) was obtained by soaking the crystalline samples of **8a** in alcohol for 7 days. In **8a**/**EtOH**, two EtOH molecules substituted two DMF molecules connected to each Ho^{3+}center (Fig. 5d), while about four lattice water molecules replaced one lattice DMF molecule filled in the pore along the *a* direction (Fig. S3†). The exchange of DMF molecules by EtOH/H_2O led to a little contraction of *b* axis (Δb = −0.47%) and small expansions of *c* axis and cell volume (Δc = 1.25%, ΔV = 0.78%) (Table S4†). The size of the square window along the *a* direction slightly increased from ca.13.51 Å × 13.51 Å to ca. 13.60 Å × 13.60 Å. The substitution of the DMF molecules by alcohol molecules led to a little shorter Ho-$O_{alcohol}$ bond distances (2.236(7) and 2.321(6) Å) in **8a**/**EtOH** (Table S6†).

It is worth to note that crystals of series B soaked in the solvents of MeOH and H_2O changed to tiny crystals not suitable for the single-crystal X-ray analyses, which may due to the high polarity of the solvents. The crystals immersed in other solvents (CH_2Cl_2, THF, diethyl ether, chloroform and acetonitrile) didn't have any changed at all, which may mainly because of the size and geometry of those solvents molecules. It is surprisingly to find that structural transformations of series A cannot happen in any of the solvent mentioned above, even when the exchange experiments were carried out at 70˚C. We speculate that this phenomenon may mainly due to the small sizes of the framework cavities in series A.

3.5 Liquid acetone sorption properties

Prompted by the reversible SCSC transformations via desolvation/solvation processes involving the acetone molecules in compound **8a**/**acetone**, we investigated the possibility to use this material as sorbents for acetone molecules in the liquid-phase. As we know, acetone is a toxic organic molecule and very harmful to human beings, and further, such a procedure can also be used to remove the acetone impurities in some organic solvents.

The acetone sorption experiments were performed as described below, and this method has been successfully used to study the liquid-phase sorption properties of other MOFs.[48] Compound **8a**/**dry** (0.1011 g, 0.0648 mmol) and a mixture of acetone and dichloromethane with a molar ratio of 1:3 (the dichloromethane was used as a reference for the calculation of the amount of absorbed acetone) were added into 2 mL $CDCl_3$. The mixture was sealed and stirred for 12 h by using magnetic stirrers. The filtrate of the resulting slurry was filtered and analyzed for the content of acetone by ^1H NMR spectroscopy. Such experiments were repeated three times and the values obtained were averaged. Details of the sorption experiments were represented in the ESI (Fig. S12†).

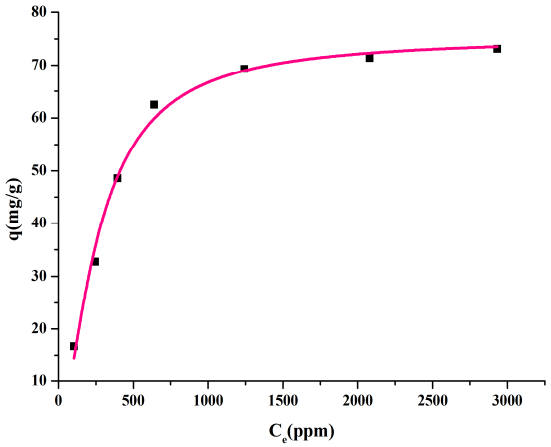

Fig. 6 Equilibrium data for the acetone sorption by **8a**/**dry** (initial acetone concentrations in the range 940–6582 ppm). The red line represents the fitting of the data with the LF model.

The acetone sorption equilibrium data are plotted in Fig. 6. The best description of the data (R^2=0.98) is provided by the Langmuir–Freundlich (LF) model. [49]

$$q = q_m \frac{(bC_e)^{\frac{1}{n}}}{1 + (bC_e)^{\frac{1}{n}}}$$

where q (mg g^{-1}) is the amount of acetone absorbed by per gram of **8a**/**dry** at the equilibrium concentration C_e (ppm of acetone remaining in solution), q_m is the maximum sorption capacity of the sorbent, b (L mg^{-1}) is the Langmuir constant related to the free energy of the sorption and n is a Freundlich constant. The results of the fitting gave the parameters q_m = 75(2) mg g^{-1}, b = 0.19(1) L g^{-1}

and n= 0.6(1). The maximum exchange capacity q_m found is consistent with the absorption of ~ 2 equivalents of per Ho^{3+} ion of **8a**/**dry**.

Furthermore, **8a**/**dry** that is used in liquid acetone sorption experiments can be easily regenerated by heating the resulted **8a**/**acetone** under vacuum at 70℃. Compound **8a**/**acetone** obtained from original and regenerated **8a**/**dry** represented almost identical PXRD patterns (Fig. S13†), which indicates the reusability of **8a**/**dry**, something that is important for practical applications.

3.6 PXRD and thermal analyses

The PXRD patterns were recorded for each series of complexes as well as the solvent exchanged complexes, and they were comparable to the corresponding simulated ones calculated from the single-crystal diffraction data (Fig. S4-S8†), indicating a pure phase of each bulky sample. To study the thermal stability of these complexes, the TGA curves of selected compounds were detected in the range of 25−800 °C (Fig. S9-S11†). Compound **8** first undergoes a weight losses of 9.08% during the temperature range of 30-253 °C, corresponding to the elimination of two free DMF and one free water molecules (calcd 9.22%). The second weight losses of 7.33% in the temperature range of 251-330 °C corresponds to the elimination of three coordinated water and one coordinated DMF molecules (calcd 7.14%). As for **8a**, the first weight losses of 12.21% within temperature range of 30-230 °C are attributed to the elimination of three free DMF and one free water molecules (calcd 12.43%). The second weight losses of 9.38%, which end at ~ 325 °C, are due to the elimination of two coordinated DMF and two coordinated water molecules (calcd 9.55%). For **8a**/**acetone**, the weight losses of 9.68% in the temperature range of 30-260 °C are due to the elimination of about three lattice water and two lattice acetone molecules (calcd 9.83%). Further weight losses up to 550°C correspond to the release of coordinated sovent molecules and decomposition of the organic ligands. For **8a**/$\mathbf{H_2O}$, the weight losses of 9.21% in the temperature range of 30-275 °C are due to the elimination of about nine lattice water molecules (calcd 9.40%). Further weight losses up to 550°C correspond to the release of coordinated sovent molecules and decomposition of the organic ligands. As for **8a**/**EtOH**, the weight losses of 11.78% in the temperature range of 30-342 °C are due to the elimination of about four lattice water and two lattice DMF molecules (calcd 11.90%). Further weight losses up to 550°C correspond to the release of coordinated sovent molecules and decomposition of the organic ligands.

3.7 Luminescence properties

The luminescent spectra of compounds **3** (Nd), **5** (Eu) and **10** (Yb) were investigated in the solid state at room temperature. Complex **5** exhibits red emission typical of Eu(III) ion upon excitation at 430 nm (the lower energy solid state absorption band) and no emission band from pamoic acid (at about 470nm) was observed (Fig. 7a), indicating that the energy transfer from the ligand to the Eu(III) center is very efficient. The transitions from the excited $^5D_0$ state to the different J levels of the lower ^7F state were observed in the emission spectrum (J= 0–4), i.e., $^5D_0 \rightarrow {}^7F_0$ at 579 nm, $^5D_0 \rightarrow {}^7F_1$ at 592 nm, $^5D_0 \rightarrow {}^7F_2$ at 613 nm, $^5D_0 \rightarrow {}^7F_3$ at 651 nm, and $^5D_0 \rightarrow {}^7F_4$ at 698 nm. The magnetic dipole transition of $^5D_0 \rightarrow {}^7F_1$ is independent of the coordination sphere, while the electric dipole transition $^5D_0 \rightarrow {}^7F_2$ emission is extremely sensitive to the nature and symmetry of coordinating environment. In a centrosymmetric environment, the magnetic dipole $^5D_0 \rightarrow {}^7F_1$ transition of Eu^{3+} is dominating, whereas distortion of the symmetry around the ion cause an intensity enhancement of the hypersensitive $^5D_0 \rightarrow {}^7F_2$ transition. The emission intensity of $^5D_0 \rightarrow {}^7F_2$ transition is much stronger than that of $^5D_0 \rightarrow {}^7F_1$ transition, indicating that Eu(III) ions locate at a low-symmetry site without inversion center, which is in good agreement with the crystal structural analysis results.[50-52]

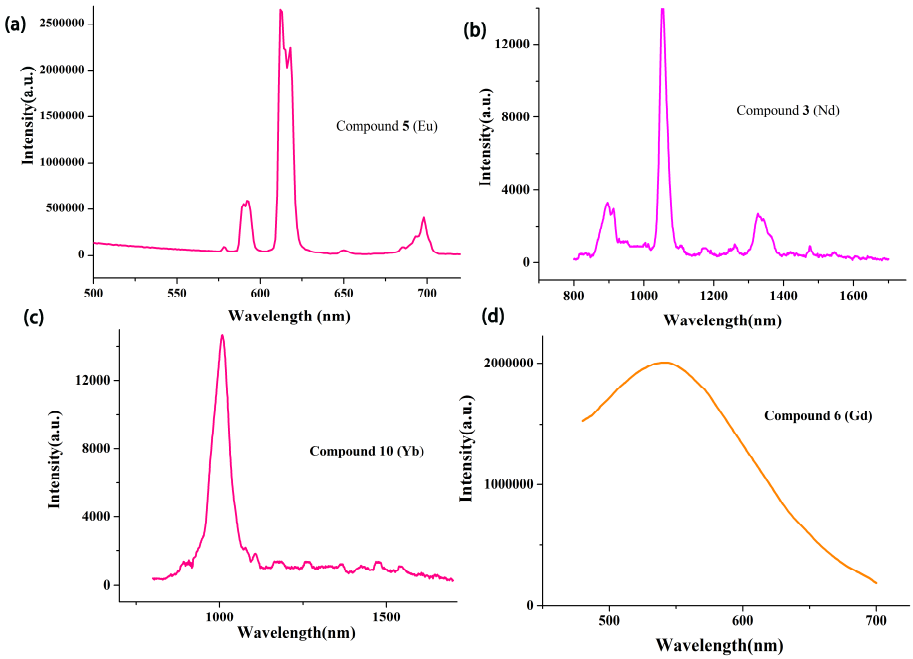

Fig. 7 The solid-state luminescent spectra of (a) compound **5**, (b) compound **3** and (c) compound **10** excited at 430 nm. (d) The phosphorescence spectrum of compound **6** (Gd).

The near-infrared (NIR) emission spectra of Nd-containing MOF **3** as well as Yb-containing MOF **10** were shown in Fig. 7b and Fig. 7c. The Nd-MOF exhibits characteristic emission of Nd(III) ion at 890, 1063 and 1330 nm, which can be attributed to the transition of $^4F_{3/2} \rightarrow {}^4I_{9/2}$, $^4F_{3/2} \rightarrow {}^4I_{11/2}$ and $^4F_{3/2} \rightarrow {}^4I_{13/2}$, respectively. The typical 1063 nm (or thereabout) sharp line which is used in a Nd:YAG laser has also been reported before in Nd-containing MOFs. [53] As shown in Fig. 7c, the Yb-MOF shows a strong emission at 980 nm resulting from the $^2F_{5/2} \rightarrow {}^2F_{7/2}$ transition upon excitation of 430 nm. [54]

As we know, the electronic transitions between the 4f orbital are forbidden on symmetry grounds and as a result the luminescence from trivalent lanthanide ions are always very week. Efficient lanthanide-centered luminescence of MOFs can be fulfilled by the use of antenna organic linkers with strong light harvesting for efficient sensitizing the lanthanide ion. Generally, the excited energy of the organic ligand undergoes an intramolecular energy transfer from the triplet state of the ligand to an excited state of the Ln^{3+} ion and then the Ln^{3+} ion typical emission occurs when the energy transfer from the lowest excited state to the ground state. Therefore, a suitable energy gap between the triplet energy level of the ligand (T1) and the radiation state of the Ln^{3+} ion is required for an optimal ligand-to-lanthanide energy transfer process. [50-51] Thus, it is necessary that the lowest triplet state of the organic linkers is located at an energy level nearly equal to or above the resonance level of the lanthanide ions. [50] Since the lowest-lying excited level of the Gd(III) ion ($^6P_{7/2}$, at 32150cm^{-1}) is too high to permit any energy transfer from the ligand to the metal center, the data obtained from the phosphorescence spectrum of the Gd^{3+} complex can actually reveal the lowest triplet energy level of the corresponding ligand. The triplet energy level of pamoic acid determined by measuring the phosphorescence spectrum of the gadolinium complex (**6**) at 77 K was found to be 18518.5 cm^{-1} (541 nm) (Fig. 7d). So, the organic linker is capable of sensitizing the trivalent ions Nd^{3+} ($^4F_{3/2}$, at 11300 cm^{-1}), Yb^{3+} ($^2F_{5/2}$, at 10200 cm^{-1}) and Eu^{3+} ($^5D_0$, at 17300 cm^{-1}) in which strong emissions have been observed in compounds **3**, **5** and **10**. No emission have been observed in the solid Tb-MOF (**7**) due to the fact that the excited state $^4D_5$ of Tb^{3+} located at

20500 cm^{-1} is too high to be sensitized by the pamoic acid. [50]

4. Conclusions

In summary, two series of new Ln-based PCPs were solvothermally synthesized under different pH values. Solvent induced dynamic behaviors of series B were investigated thoroughly through SCSC transformations. The capability of activated series B to absorb liquid acetone was evaluated by means of ^1H NMR spectroscopy, demonstrating the potential of Ln-MOFs as highly efficient and reusable liquid acetone sorbents. Photoluminescence property studies of the selected compounds in series A indicate that pamoic acid was a promising emission sensitizer for Nd^{3+}, Eu^{3+} and Yb^{3+}. Further studies concerning the adjustable magnetic, ferroelectric and luminescence properties triggered by the solvent-exchange structural transformations are underway in our lab, with the aim of exploring interesting materials for potential applications.

Acknowledgements

This work was funded by the National Natural Science Foundation of China (No. 21371154).

†**Electronic supplementary information** (ESI) available: X-ray crystallographic files in CIF format; the additional structures and characterizations, figures and tables, etc.

References

1 J. R. Li, J. Sculley, H. C. Zhou, *Chem. Rev*., 2012, **112**, 869.

2 S. Ma, H. C. Zhou, *Chem. Commun*., 2010, **46**, 44.

3 J. Sculley, D. Yuan, H. C. Zhou, *Energy Environ. Sci*., 2011, **4**, 2721.

4 L. J. Murray, M. Dinca, J. R. Long, *Chem. Soc. Rev*., 2009, **38**, 1294.

5 J. L. C. Rowsell, O. M. Yaghi, *Angew. Chem., Int. Ed*., 2005, **44**, 4670.

6 R. C. Huxford, J. D. Rocca, W. B. Lin, *Curr. Opin. Chem. Biol*., 2010, **14**, 262.

7 J. D. Rocca, D. M. Liu, W. B. Lin, *Acc. Chem. Res*., 2011, **44**, 957.

8 P. Horcajada, R. Gref, T. Baati, P. K. Allan, G. Maurin, P. Couvreur, G. Ferey, R. E. Morris, C. Serre, *Chem. Rev*., 2012, **112**, 1232.

9 J. Lee, O. K. Farha, J. Roberts, K. A. Scheidt, S. T. Nguyen, J. T. Hupp, *Chem. Soc. Rev.*, 2009, **38,** 1450.

10 D. Farrusseng, S. Aguado, C. Pinel, *Angew. Chem., Int. Ed*., 2009, **48**, 7502.

11 A. Corma, H. García, F. X. Llabrés i Xamena, *Chem. Rev*., 2010, **110**, 4606.

12 J. Rocha, L. D. Carlos, F. A. Almeida Paz, D. Ananias, *Chem. Soc. Rev.*, 2011, **40**, 926.

13 M. D. Allendorf, C. A.Bauer, R. K. Bhakta, R. J. T. Houk, *Chem. Soc. Rev*., 2009, **38**, 1330.

14 B. Chen, S. Xiang, G. Qian, *Acc. Chem. Res*., 2010, **43**, 1115.

15 E. Y. Cho, J. M. Gu, I. H. Choi, W. S. Kim, Y. K. Hwang, S. Huh, S.-J. Kim, Y. Kim, *Cryst. Growth Des.*, 2014, **14**, 5026.

16 W. Yang, Z. Q. Bai, W. Q. Shi, L. Y. Yuan, T. Tian, Z. F. Chai, H. Wang, Z. M. Sun, *Chem. Commun*., 2013, **49**, 10415.

17 R. W. Larsen, L. Wojtas, J. Perman, R. L. Musselman, M. J. Zaworotko, C. M. Vetromile, *J. Am. Chem. Soc*., 2011, **133**, 10356.

18 S. V. Potts, L. J. Barbour, D. A. Haynes, J. M. Rawson, G. O. Lloyd, *J. Am. Chem. Soc*., 2011, **133**, 12948.

19 B. Li, Y. Zhang, D. Ma, T. Ma, Z. Shi, S. Ma, *J. Am. Chem. Soc*., 2014, **136**, 1202.

20 S. Horike, S. Shimomura, S. Kitagawa, *Nat. Chem.*, 2009, **1**, 695.

21 G. Mukherjee, K. Biradha, *Chem. Commun.*, 2014, **50**, 670.

22 Y. C. He, J. Yang, Y. Y. Liu, J. F. Ma, *Inorg. Chem*., 2014, **53**, 7527.

23 L. Liu, X. Q. Wang, A. J. Jacobson, *Dalton Trans.*, 2010, **39**, 1722.

24 J. R. Li, J. Yu, W. Lu, J. Sculley, P. B. Balbuena, H. C. Zhou, *Nat. Commun*., 2013, **4**, 1538.

25 M. P. Suh, H. J. Park, T. K. Prasad, D. W. Lim, *Chem. Rev*., 2012, **112**, 782.

26 D. S. Zhang, Z. Chang, Y. F. Li, Z. Y. Jiang, Z. H. Xuan, Y. H. Zhang, J. R. Li, Q. Chen, T. L. Hu, X. H. Bu, *Sci. Rep*., 2013, **3**, 3312.

27 R. Medishetty, L. L. Koh, G. K. Kole, J. J. Vittal, *Angew. Chem., Int. Ed*., 2011, **50**, 10949.

28 Q. K. Liu, J. P. Ma, Y. B. Dong, *Chem. Commun*., 2011, **47**, 12343.

29 B. Tsolmon, F. Sun, J. Zhang, J. Cai, H. Ren, G. Zhu, *Chem. Commun*., 2012, **48**, 7613.

30 J. Li, P. Huang, X. R. Wu, J. Tao, R. B. Huang, L. S. Zheng, *Chem. Sci*., 2013, **4**, 3232.

31 W. M. Bloch, C. J. Sumby, *Chem. Commun*., 2012, **48**, 2534.

32 M. L. Foo, R. Matsuda, S. Kitagawa, *Chem. Mater*., 2014, **26**, 310.

33 Y. Cui, H. Xu, Y. Yue, Z. Guo, J. Yu, Z. Chen, J. Gao, Y. Yang, G. Qian, B. Chen, *J. Am. Chem. Soc*., 2012, **134**, 3979.

34 Y. B. He, S. C. Xiang, Z. J. Zhang, S. S. Xiong, F. R. Fronczek, R, Krishna, M. O'Keeffe and B. L. Chen, *Chem. Commun*., 2012, **48**, 10856.

35 R. Singh, J. Mrozinski, P. K. Bharadwa, *Cryst. Growth Des*., 2014, **14**, 3623.

36 S. Neogi, S. Sen, P. K. Bharadwaj, *CrystEngComm*, 2013, **15**, 9239.

37 P. K. Allan, B. Xiao, S. J. Teat, J. W. Knight, R. E. Morris, *J. Am. Chem. Soc*., 2010, **132**, 3605.

38 K. Kuriki, Y. Koike, Y. Okamoto, *Chem. Rev*., 2002**, 102**, 2347.

39 J. C. G. Bünzli, C. Piguet, *Chem. Soc. Rev*., 2005, **34**, 1048.

40 J. Xu, J. W. Cheng, W. P. Su, M. C. Hong, *Cryst. Growth Des*., 2011, **11**, 2294.

41 (*a*) L. N. Zhang, S. T. Lu, C. Zhang, C. X. Du and H. W. Hou, *CrystEngComm*, 2015, **17**, 846; (*b*) S. Biswas, H. S. Jena, S. Goswami, S. Sanda and S. Konar, *Cryst. Growth Des.*, 2014, **14**, 1287.

42 G. M. Sheldrick, *SHELXS-97*, *Program for Crystal Structure Solution*, University of Göttingen, Göttingen, Germany, 1997.

43 G. M. Sheldrick, *SHELXL-97*, *Program for Crystal Structure Refinement*, University of Göttingen, Göttingen, Germany, 1997.

44 A. L. Spek, *J. Appl. Crystallogr.*, 2003, **36**, 7.

45 K. N. Raymond, D. L. Wellman, C. Sgarlata, A. P. Hill, *C. R. Chim*., 2010, **13**, 849.

46 R. D. Shannon, *Acta Crystallogr*., 1976, **A32**, 751.

47 Q. Gao, X. Wang, A. J. Jacobson, *Inorg. Chem*., 2011, **50**, 9073.

48 C. G. Efthymiou, E. J. Kyprianidou, C. J. Milios, M. J. Manos, A. J. Tasiopoulos, *J. Mater. Chem. A*., 2013, **1**, 5061.

49 M. J.Manos, M. G. Kanatzidis, *J. Am. Chem. Soc*., 2012, **134**, 16441.

50 Y. J. Cui, Y. F. Yue, G. D. Qian, B. L. Chen, *Chem. Rev*., 2012, **112**, 1126.

51 B. Zhang, T. Xiao, C. M. Liu, Q. Li, Y. Y. Zhu, M. S. Tang, C. X. Du, and M. P. Song, *Inorg. Chem*., 2013, **52**, 13332.

52 X. Wang, Q. G. Zhai, S. N. Li, Y. C. Jiang, M. C. Hu, *Cryst. Growth Des*., 2014, **14,** 177.

53 R. Decadt, K. V. Hecke, D. Depla, K. Leus, D. Weinberger, I. V. Driessche, P. V. D. Voort, R. V. Deun, *Inorg. Chem*., 2012, **51**, 11623.

54 X. J. Zheng, A. Ablet, C. Ng, W. T. Wong, *Inorg. Chem*., 2014, **53**, 6788.